STANFORD
AERONAUTICS &
ASTRONAUTICS

# Introduction to Symmetry Analysis

## Chapter 11 - Incompressible Flow

Brian Cantwell
Department of Aeronautics and Astronautics
Stanford University

STANFORD
AERONAUTICS &
ASTRONAUTICS

# Symmetries of the Navier Stokes Equations

$$\frac{\partial u^j}{\partial x^j} = 0, \quad \text{(sum over } j = 1, 2, 3),$$

$$\frac{\partial u^i}{\partial t} + u^j \frac{\partial u^i}{\partial x^j} + \frac{\partial p}{\partial x^i} - \nu \frac{\partial^2 u^i}{\partial x^j \partial x^j} = 0, \qquad i = 1, 2, 3, \tag{11.1}$$

sum over $j = 1, 2,$

Infinitesimal transformation

$$\begin{aligned} \tilde{x}^i &= x^i + s\xi^i[\boldsymbol{x}, t], \\ \tilde{t} &= t + s\tau[\boldsymbol{x}, t], \\ \tilde{u}^i &= u^i + s\eta^i[\boldsymbol{x}, t], \\ \tilde{p} &= p + s\zeta[\boldsymbol{x}, t]. \end{aligned}$$

STANFORD
AERONAUTICS &
ASTRONAUTICS

(1) Invariance under translation in time:

$$X^1 = \frac{\partial}{\partial t}. \tag{11.3}$$

(2) An arbitrary function of time, $g[t]$, added to the pressure:

$$X^2 = g[t]\frac{\partial}{\partial p}. \tag{11.4}$$

(3) Rotation about the $z$-axis:

$$X^3 = y\frac{\partial}{\partial x} - x\frac{\partial}{\partial y} + v\frac{\partial}{\partial u} - u\frac{\partial}{\partial v}. \tag{11.5}$$

(4) Rotation about the $x$-axis:

$$X^4 = z\frac{\partial}{\partial y} - y\frac{\partial}{\partial z} + w\frac{\partial}{\partial v} - v\frac{\partial}{\partial w}. \tag{11.6}$$

(5) Rotation about the $y$-axis:

$$X^5 = z\frac{\partial}{\partial x} - x\frac{\partial}{\partial z} + w\frac{\partial}{\partial u} - u\frac{\partial}{\partial w}. \tag{11.7}$$

(6) Nonuniform translation in the $x$-direction:

$$X^6 = a[t]\frac{\partial}{\partial x} + \left(\frac{da}{dt}\right)\frac{\partial}{\partial u} - x\left(\frac{d^2a}{dt^2}\right)\frac{\partial}{\partial p}. \tag{11.8}$$

$a[t]$ is an arbitrary, twice differentiable function of time. Simple translation in $x$ corresponds to $a[t] = \text{const}$.

(7) Nonuniform translation in the $y$-direction:

$$X^7 = b[t]\frac{\partial}{\partial y} + \left(\frac{db}{dt}\right)\frac{\partial}{\partial v} - y\left(\frac{d^2b}{dt^2}\right)\frac{\partial}{\partial p}. \tag{11.9}$$

$b[t]$ is an arbitrary, twice differentiable function.

(8) Nonuniform translation in the $z$-direction:

$$X^8 = c[t]\frac{\partial}{\partial z} + \left(\frac{dc}{dt}\right)\frac{\partial}{\partial w} - z\left(\frac{d^2c}{dt^2}\right)\frac{\partial}{\partial p}. \tag{11.10}$$

$c[t]$ is an arbitrary, twice differentiable function.

(9) The one-parameter dilation group of the equation

$$X^9 = 2t\frac{\partial}{\partial t} + x\frac{\partial}{\partial x} + y\frac{\partial}{\partial y} + z\frac{\partial}{\partial z} - u\frac{\partial}{\partial u} - v\frac{\partial}{\partial v} - w\frac{\partial}{\partial w} - 2p\frac{\partial}{\partial p}. \tag{11.11}$$

The equations are invariant under a 9-parameter group of translations, rotations and dilations

STANFORD
AERONAUTICS &
ASTRONAUTICS

One-parameter dilation group of the full viscous equations.

$$\tilde{x}^i = e^s x^i,$$
$$\tilde{t} = e^{2s} t,$$
$$\tilde{u}^i = e^{-s} u^i,$$
$$\tilde{p} = e^{-2s} p.$$

If the kinematic viscosity is set to zero, the resulting Euler equations are invariant under a two-parameter dilation group.

$$\tilde{x}^i = e^s x^i,$$
$$\tilde{t} = e^{s/k} t,$$
$$\tilde{u}^i = e^{s(1-1/k)} u^i,$$
$$\tilde{p} = e^{s(2-2/k)} p$$

STANFORD
AERONAUTICS &
ASTRONAUTICS

In addition the equations are invariant under a group of arbitrary translations in space.

$$\tilde{x}^j = x^j + a^j[t],$$
$$\tilde{t} = t,$$
$$\tilde{u}^i = u^i + \frac{da^i}{dt},$$
$$\tilde{p} = p - x^j \frac{d^2 a^j}{dt^2} + g[t].$$

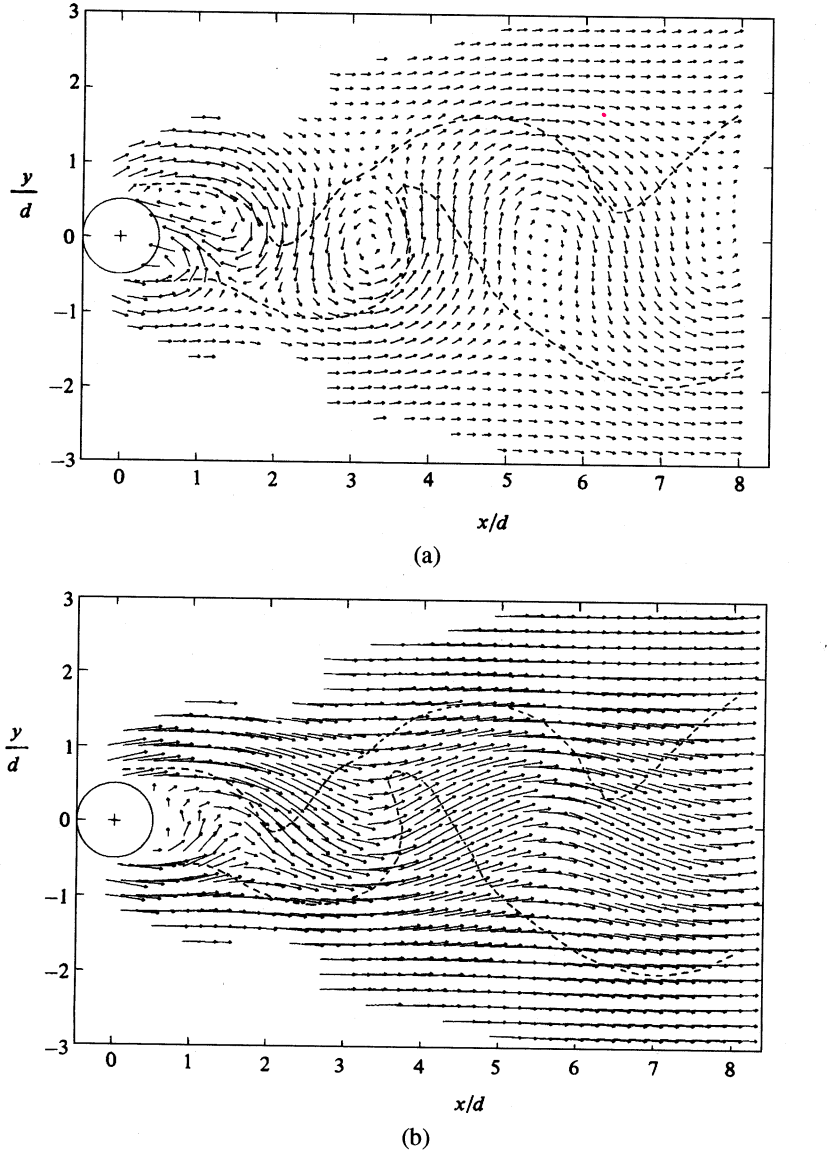


Fig. 11.1. Velocity vector field in the wake of a circular cylinder from Reference [11.6] as viewed by two observers: (a) frame of reference moving downstream at $0.755U_\infty$, (b) frame of reference fixed with respect to the cylinder. The dashed contour roughly corresponds to the instantaneous boundary of turbulence.

Instantaneous flow field in the wake of a circular cylinder as seen by two observers.

STANFORD
AERONAUTICS &
ASTRONAUTICS

# The impulse integral – Conservation of Momentum in an Infinite Domain

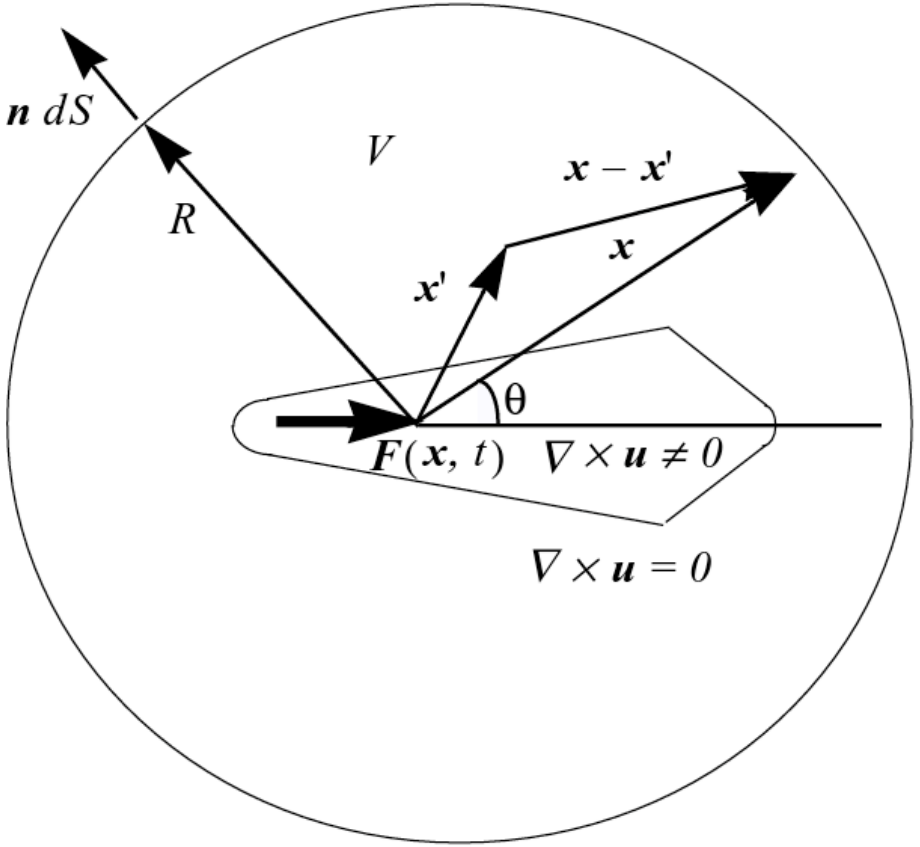


Fig. 11.3. Spherical control volume surrounding a force distribution in a viscous fluid.

The vorticity is related to the vector potential by a Poisson equation.

$$\boldsymbol{\omega} = -\boldsymbol{\nabla}^2 \boldsymbol{A}. \tag{11.51}$$

The general solution is

$$\boldsymbol{A}[\boldsymbol{x}, t] = \frac{1}{4\pi} \int_V \frac{\boldsymbol{\omega}[\boldsymbol{x}', t]}{|\boldsymbol{x} - \boldsymbol{x}'|} \, d\boldsymbol{x}', \tag{11.52}$$

where $d\boldsymbol{x}'$ is a volume element in $\boldsymbol{V}$.

We want to work out the volume integrated momentum.

$$\boldsymbol{H}[t] = \int_V \boldsymbol{u}[\boldsymbol{x}, t]\, d\boldsymbol{x}, \tag{11.53}$$

The volume integral can be expressed as a surface integral of the vector potential.

$$\boldsymbol{H}[t] = \int_S \boldsymbol{n} \times \boldsymbol{A}[\boldsymbol{x}, t]\, dS = \boldsymbol{R}^2 \int_S \frac{\boldsymbol{x}}{\boldsymbol{R}} \times \boldsymbol{A}[\boldsymbol{x}, t]\, d\Omega, \tag{11.54}$$

where

$$\boldsymbol{n} = \frac{\boldsymbol{x}}{\boldsymbol{R}} = \boldsymbol{i} \sin\theta \cos\phi + \boldsymbol{j} \sin\theta \sin\phi + \boldsymbol{k} \cos\theta, \tag{11.55}$$

and $d\Omega$ is an infinitesimal solid angle, $d\Omega = \sin\theta\, d\theta\, d\phi$.

Make use of

$$\int_S \frac{\boldsymbol{x}}{|\boldsymbol{x}-\boldsymbol{x}'|}\, d\Omega = \frac{4\pi}{3}\left(\frac{\boldsymbol{x}}{\boldsymbol{R}}\right), \tag{11.56}$$

to obtain

$$\boxed{\boldsymbol{H}[t] = \tfrac{2}{3}\boldsymbol{I}[t],} \tag{11.57}$$

where

$$\boldsymbol{I}[t] = \frac{1}{2}\int_V \boldsymbol{x} \times \boldsymbol{\omega}[\boldsymbol{x}, t]\, d\boldsymbol{x} \tag{11.58}$$

STANFORD
AERONAUTICS &
ASTRONAUTICS

Use a control volume balance of the momentum equation to evaluate the impulse integral.

$$\frac{\partial \boldsymbol{u}}{\partial t} + \boldsymbol{\nabla} \cdot (\boldsymbol{u}\boldsymbol{u}) + \boldsymbol{\nabla}\left(\frac{p}{\rho}\right) - \nu \boldsymbol{\nabla}^2 \boldsymbol{u} = \frac{\boldsymbol{F}[\boldsymbol{x}, t]}{\rho}. \qquad (11.59)$$

Note

$$\boldsymbol{\nabla} \times \boldsymbol{\nabla} \times \boldsymbol{u} = \boldsymbol{\nabla}(\boldsymbol{\nabla} \cdot \boldsymbol{u}) - \boldsymbol{\nabla}^2 \boldsymbol{u} \qquad (11.60)$$

$$\boldsymbol{\nabla} \cdot \boldsymbol{u} = 0$$

$$\frac{\partial \boldsymbol{u}}{dt} + \boldsymbol{\nabla} \cdot (\boldsymbol{u}\boldsymbol{u}) + \boldsymbol{\nabla}\left(\frac{p}{\rho}\right) + \nu \boldsymbol{\nabla} \times \boldsymbol{\omega} = \frac{\boldsymbol{F}[\boldsymbol{x}, t]}{\rho}. \qquad (11.61)$$

STANFORD
AERONAUTICS &
ASTRONAUTICS

Integrate

$$\frac{d\boldsymbol{H}}{dt} + \int_S \left( \boldsymbol{uu} + \frac{p}{\rho}\boldsymbol{I} \right) \cdot \boldsymbol{n}\, dS + \nu \int_S (\boldsymbol{\omega} \times \boldsymbol{n})\, dS = \int_V \frac{\boldsymbol{F}[\boldsymbol{x}, t]}{\rho}\, dV. \tag{11.62}$$

$$\frac{d\boldsymbol{H}}{dt} + \int_S \left( \boldsymbol{uu} + \frac{p}{\rho}\boldsymbol{I} \right) \cdot \boldsymbol{n}\, dS = \int_V \frac{\boldsymbol{F}[\boldsymbol{x}, t]}{\rho}\, dV. \tag{11.63}$$

At large distance from the force the vector potential can be expressed in terms of a multipole expansion.

$$\boldsymbol{A} = \frac{\boldsymbol{q}}{4\pi r} + \frac{\boldsymbol{Q} \cdot \boldsymbol{x}}{4\pi r^3} + O\left( \frac{1}{r^3} \right), \tag{11.64}$$

where

$$\boldsymbol{q} = -\int_V \boldsymbol{\omega}[\boldsymbol{x}', t]\, d\boldsymbol{x}', \qquad \boldsymbol{Q} = -\int_V \boldsymbol{\omega}[\boldsymbol{x}', t]\boldsymbol{x}'\, d\boldsymbol{x}'. \tag{11.65}$$

$$\boldsymbol{Q}\cdot\boldsymbol{x} = -\boldsymbol{x}\times\left(\frac{1}{2}\int_V \boldsymbol{x}'\times\boldsymbol{\omega}[\boldsymbol{x}',t]\,d\boldsymbol{x}'\right). \tag{11.66}$$

To lowest order

$$\boldsymbol{A} = \frac{1}{4\pi}\frac{\boldsymbol{I}[t]\times\boldsymbol{x}}{r^3} + O\left(\frac{1}{r^3}\right). \tag{11.67}$$

These results for the far-field vector potential have a direct analogy with magnetostatics. The velocity $\boldsymbol{u}$ is analogous to the magnetic field, and the vorticity $\boldsymbol{\omega}/4\pi$ is analogous to the current density. Jackson [11.16] provides an excellent reference in this connection. Using (11.67), we can estimate the surface integral of the nonlinear term in (11.63) as

$$\int_S (\boldsymbol{uu}) \cdot \boldsymbol{n}\, dS \sim \frac{1}{\boldsymbol{R}^4} \qquad \text{as} \quad R \to \infty. \tag{11.68}$$

$$\frac{d\boldsymbol{H}}{dt} + \int_S \left(\frac{p}{\rho}\right)\boldsymbol{n}\, dS = \int_V \frac{\boldsymbol{F}[\boldsymbol{x}, t]}{\rho}\, dV \tag{11.69}$$

We can derive an expression for the far field pressure

$$\frac{\partial \boldsymbol{u}}{\partial t} + \frac{1}{\rho}\boldsymbol{\nabla} p = 0. \tag{11.70}$$

Far field vector potential

$$\boldsymbol{A} = \frac{1}{4\pi}\frac{\boldsymbol{I}[t] \times \boldsymbol{x}}{r^3} + O\left(\frac{1}{r^3}\right). \tag{11.67}$$

Far field velocity

$$\boldsymbol{u} = -\frac{1}{4\pi}\boldsymbol{\nabla}\left(\frac{\boldsymbol{I} \cdot \boldsymbol{x}}{r^3}\right). \tag{11.71}$$

where we have used

$$\boldsymbol{\nabla} \cdot (\boldsymbol{x}/r^3) = \boldsymbol{\nabla} \times (\boldsymbol{x}/r^3) = 0.$$

STANFORD
AERONAUTICS &
ASTRONAUTICS

# Summary – overall conservation of momentum

$$\boldsymbol{H}[t] = \int_V \boldsymbol{u}[\boldsymbol{x}, t]\, d\boldsymbol{x}, \tag{11.53}$$

$$\lim_{R\to\infty} \left(\frac{p}{\rho}\right) = \frac{1}{4\pi}\left(\frac{d\boldsymbol{I}}{dt}\right) \cdot \frac{\boldsymbol{x}}{r^3}. \tag{11.72}$$

$$\boxed{\int_S \left(\frac{p}{\rho}\right)\boldsymbol{n}\, dS = \frac{1}{3}\frac{d\boldsymbol{I}[t]}{dt}.} \tag{11.73}$$

$$\boxed{\boldsymbol{H}[t] = \tfrac{2}{3}\boldsymbol{I}[t],} \tag{11.57}$$

$$\boldsymbol{I}[t] = \int_0^t \int_V \frac{\boldsymbol{F}[\boldsymbol{x}, t]}{\rho}\, dx\, dt. \tag{11.74}$$

STANFORD
AERONAUTICS &
ASTRONAUTICS

# The Impulsively Started Round Jet

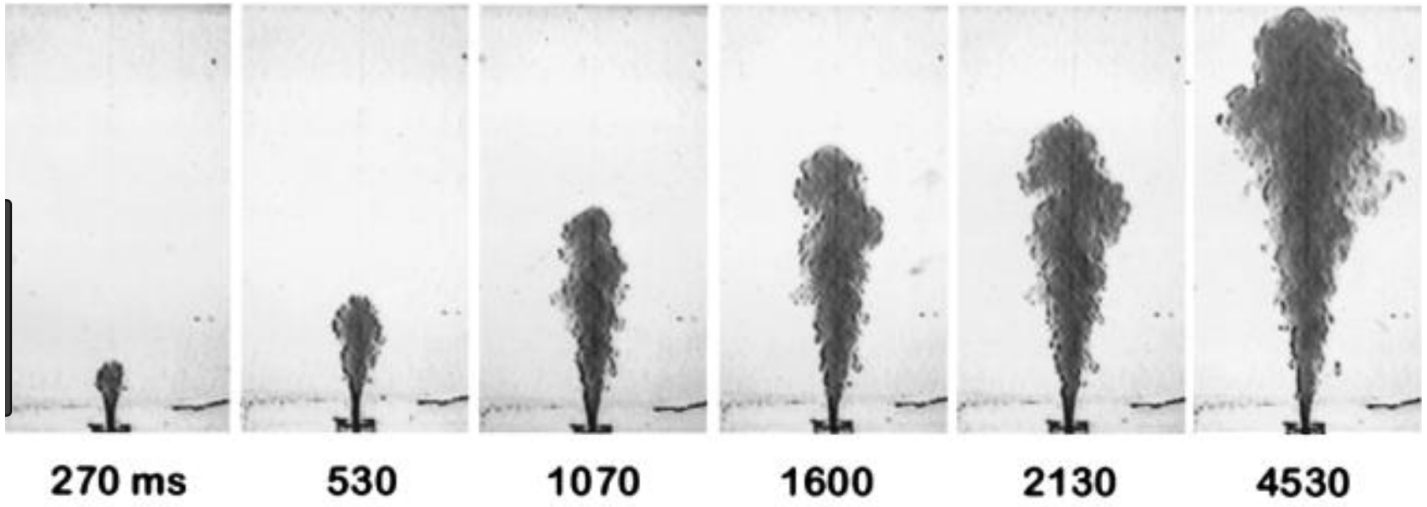


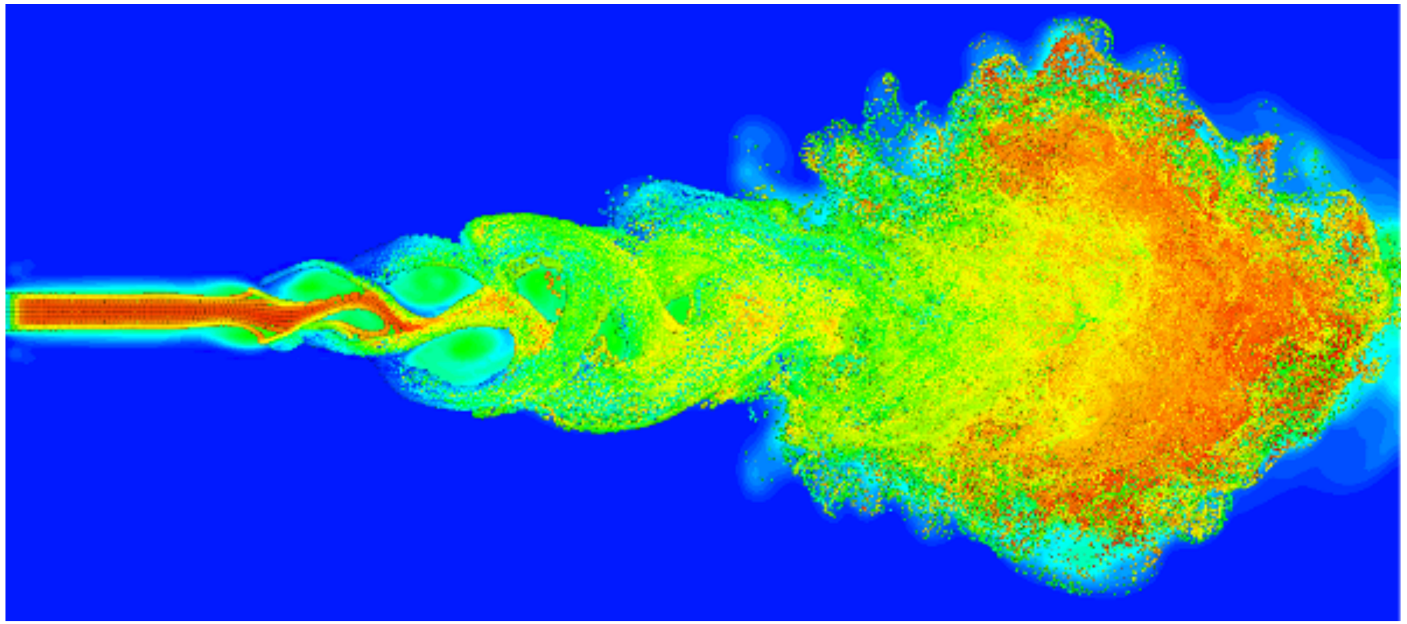

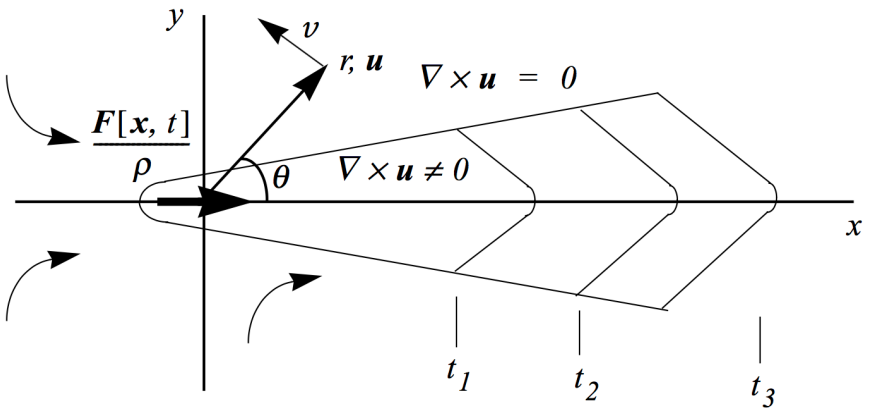


Fig. 11.4. Schematic of the unsteady propagation of a started jet. The boundary schematically delineates the regions of rotational and irrotational flow.

Figure 11.4 schematically shows the development of the vorticity-bearing region of an unsteady jet at several successive times. The jet is produced by a point force acting impulsively in a fluid that is initially everywhere at rest. The force distribution is of the form

$$\frac{\boldsymbol{F}[\boldsymbol{x}, t]}{\rho} = \frac{J}{\rho} h[t]\delta[x]\delta[y]\delta[z], \tag{11.75}$$

where $h[t]$ is the Heaviside function,

$$h[t] = \begin{cases} 0, & t < 0, \\ 1, & t > 0, \end{cases} \tag{11.76}$$

$\delta[x]$ is the Dirac delta function and J is the amplitude of the force directed along the x-axis. Using (11.57) and (11.73), the impulse integral is

$$\int_V \boldsymbol{u}[\boldsymbol{x}, t]\, dx = \frac{2}{3}\left(\frac{J}{\rho}\right) t, \tag{11.77}$$

indicating that the total momentum of the fluid grows linearly with time.

# Symmetry Group

Now let's show that this problem is invariant under the fundamental dilation group of the Navier–Stokes equations,

$$\begin{aligned} \tilde{x}^i &= e^a x^i, & \tilde{t} &= e^{2a} t, \\ \tilde{u}^i &= e^{-a} u^i, & \frac{\tilde{p}}{\rho} &= e^{-2a} \frac{p}{\rho}, \\ \tilde{\omega} &= e^{-2a} \omega, & \tilde{\psi} &= e^a \psi. \end{aligned} \tag{11.78}$$

Note that $\psi$ in (11.78) is the Stokes stream function with dimensions $\hat{\psi} = L^3/T$. The invariance is confirmed by transforming the impulse integral

$$\begin{aligned} \int_V \tilde{\boldsymbol{u}}\, d\tilde{\boldsymbol{x}} = \frac{2}{3}\left(\frac{J}{\rho}\right)\tilde{t} \Rightarrow e^{2a}\int_V \boldsymbol{u}\, d\boldsymbol{x} &= e^{2a}\frac{2}{3}\left(\frac{J}{\rho}\right)t \\ \Rightarrow \int_V \boldsymbol{u}\, d\boldsymbol{x} &= \frac{2}{3}\left(\frac{J}{\rho}\right)t. \end{aligned} \tag{11.79}$$

The Reynolds number

$$\boxed{Re = \frac{(J/\rho)^{1/2}}{\nu}}$$

### 11.5.2.1 Governing Equations

The problem is most conveniently formulated in spherical polar coordinates, and the governing equations in in these variables are

$$\frac{1}{r}\frac{\partial(r^2 u)}{\partial r} + \frac{1}{\sin\theta}\frac{\partial(v\sin\theta)}{\partial\theta} = 0, \qquad \text{(continuity)},$$

$$\frac{\partial(rv)}{\partial r} - \frac{\partial u}{\partial\theta} = r\omega \qquad \text{(vorticity)},$$

$$\frac{\partial(r\omega)}{\partial t} + \frac{\partial(ru\omega)}{\partial r} + \frac{\partial(v\omega)}{\partial\theta} = \nu\left(\frac{1}{r}\frac{\partial}{\partial\theta}\left(\frac{1}{\sin\theta}\frac{\partial(\omega\sin\theta)}{\partial\theta}\right) + \frac{\partial^2(r\omega)}{\partial r^2}\right)$$

(momentum). (11.81)

The Stokes stream function is introduced to integrate the continuity equation:

$$u = \frac{1}{r^2\sin\theta}\frac{\partial\psi}{\partial\theta}, \qquad v = \frac{-1}{\sin\theta}\frac{\partial\psi}{\partial r}. \tag{11.82}$$

Note that the dimensions of $\psi$ in (11.82) are $L^3/T$, whereas for the stream function in 2-D flow the units are $L^2/T$. We are primarily concerned with the ODEs governing particle paths,

$$\frac{dr}{dt} = u[r,\theta,t], \qquad \frac{d\theta}{dt} = \frac{v[r,\theta,t]}{r}, \tag{11.83}$$

where the jet is directed along the polar axis and the velocity components, $u$ and $v$, are in the radial and tangential directions respectively. See Figure 11.4. The group (11.78) can be cast in spherical polar coordinates (the transformations of

the radius and angle are simply $\tilde{r} = e^a r$, $\tilde{\theta} = \theta$), and the characteristic equations are

$$\frac{dr}{r} = \frac{d\theta}{0} = \frac{dt}{2t} = \frac{du}{-u} = \frac{dv}{-v} = \frac{d(p/\rho)}{-2p/\rho} = \frac{d\omega}{-2\omega} = \frac{d\psi}{\psi}. \quad (11.84)$$

All the relevant similarity variables are generated as the integrals of (11.84):

$$\begin{aligned} \xi &= r/(\nu t)^{1/2}, \\ \theta &= \theta, \\ U[\xi, \theta] &= \frac{u t^{1/2}}{\nu^{1/2}}, \\ V[\xi, \theta] &= \frac{v t^{1/2}}{\nu^{1/2}}, \\ P[\xi] &= \left(\frac{p}{\rho}\right)\frac{t}{\nu}, \\ \Omega[\xi, \theta] &= \omega t, \\ \Psi[\xi, \theta] &= \frac{\psi}{\nu^{3/2} t^{1/2}}. \end{aligned} \quad (11.85)$$

Upon substitution of (11.85), the equations of motion (11.81) become

$$\begin{aligned}
\frac{1}{\xi}\frac{\partial(\xi^2 U)}{\partial \xi} + \frac{1}{\sin\theta}\frac{\partial(V\sin\theta)}{\partial\theta} &= 0 \qquad \text{(continuity)},\\
\frac{\partial(\xi V)}{\partial\xi} - \frac{\partial U}{\partial\theta} &= \xi\Omega \qquad \text{(vorticity)},\\
\frac{\partial}{\partial\xi}\left(\left(U - \frac{\xi}{2}\right)\xi\Omega\right) + \frac{\partial(V\Omega)}{\partial\theta} &= \frac{1}{\xi}\frac{\partial}{\partial\theta}\left(\frac{1}{\sin\theta}\frac{\partial(\Omega\sin\theta)}{\partial\theta}\right)\\
&\quad + \frac{\partial^2(\xi\Omega)}{\partial\xi^2} \qquad \text{(momentum)},
\end{aligned} \tag{11.86}$$

and the self-similar velocities are

$$U = \frac{1}{\xi^2\sin\theta}\frac{\partial\psi}{\partial\theta}, \qquad V = \frac{-1}{\sin\theta}\frac{\partial\psi}{\partial\xi}. \tag{11.87}$$

The particle path equations (11.83) become

$$\frac{\partial\xi}{d\tau} = U[\xi,\ \theta; Re] - \frac{\xi}{2}, \qquad \frac{d\theta}{d\tau} = \frac{V[\xi,\ \theta;\ Re]}{\xi}, \tag{11.88}$$

where $\tau = \ln[t]$.

### *11.5.2.2 Critical Points in Three Dimensions*

Much of the analysis that follows will focus on the various vector field patterns of (11.88) and on the critical points $(\xi_c, \theta_c)$; we have

$$\begin{aligned} U[\xi_c, \theta_c; Re] - \frac{\xi_c}{2} &= 0, \\ \frac{V[\xi_c, \theta_c; Re]}{\xi_c} &= 0, \end{aligned} \tag{11.89}$$

where the parametric dependence of the velocity field on the Reynolds number is indicated. One of the most important aspects of this approach is that structural features of the flow, which are not visible in the streamline pattern, become evident in the pattern of particle trajectories.

The analysis of the critical points of (11.88) is carried out using the theory developed in Chapter 3, Section 3.9.4. For this purpose it is easier to work with the particle path equations in Cartesian coordinates,

$$\frac{dx^i}{dt} = u^i(\boldsymbol{x}, t) \Rightarrow \frac{d\xi^i}{d\tau} = U^i[\boldsymbol{\xi}; Re] - \frac{\xi^i}{2}. \tag{11.90}$$

where $\xi^i = x^i/\sqrt{\nu t}$.

The character of a critical point is determined by expanding the flow in a Taylor series near the critical point and truncating at first order:

$$\frac{d\xi^i}{d\tau} = \left(A^i_j - \frac{1}{2}\delta^i_j\right)\Big|_{\boldsymbol{\xi}=\boldsymbol{\xi}_c} \left(\xi^j - \xi^j_c\right). \tag{11.91}$$

The similarity form of the velocity gradient tensor is

$$a^i_j = \frac{\partial u^i}{\partial x^j} = \frac{1}{t}\frac{\partial U^i}{\partial \xi^j} = \frac{1}{t}A^i_j[\boldsymbol{\xi}]. \tag{11.92}$$

Note that the value of the dimensioned velocity gradient tensor does not depend on $J/\rho$ or $\nu$. Therefore an observer moving at a fixed $\boldsymbol{\xi}$ can use the current value of the velocity gradient as a local clock to determine the global age of the flow, regardless of the flow Reynolds number.

The nature of the critical point is determined by the invariants of the matrix

$$M^i_j = A^i_j - \tfrac{1}{2}\delta^i_j \tag{11.93}$$

in (11.91) evaluated at the critical point. The first invariants of $A$ and $M$ are

$$P_M = \tfrac{3}{2}, \qquad P_A = 0. \tag{11.94}$$

The second and third invariants $(Q, R)$ are expressed in terms of matrix elements

$$\begin{aligned} Q_A &= -\tfrac{1}{2}A^i_k A^k_i, \\ Q_M &= \tfrac{9}{8} - \tfrac{1}{2}M^i_k M^k_i \end{aligned} \tag{11.95}$$

and

$$\begin{aligned} R_A &= -\tfrac{1}{3}A^i_k A^k_j A^j_i, \\ R_M &= -\tfrac{1}{3}M^i_k M^k_j M^j_i - \tfrac{3}{2}Q_M + \tfrac{27}{24}. \end{aligned} \tag{11.96}$$

The invariants of $M$ and $A$ are related to one another as follows

$$\begin{aligned} Q_M &= Q_A + \tfrac{3}{4}, \\ R_M &= R_A + \tfrac{1}{2}Q_A + \tfrac{1}{8}. \end{aligned} \tag{11.97}$$

The discriminant of $A$ is

$$D_A = Q_A^3 + \tfrac{27}{4}R_A^2, \tag{11.98}$$

and the discriminant of $M$ is

$$D_M = Q_M^3 + \tfrac{27}{4}R_M^2 + \tfrac{27}{4}R_M\left(\tfrac{1}{2} - Q_M\right) - \tfrac{9}{16}Q_M^2. \tag{11.99}$$

STANFORD
AERONAUTICS &
ASTRONAUTICS

*11.5.2.5 The Limit $Re \to 0$*

If one takes the limit of (11.104) as $Re \to 0 (A \to \infty)$, the result is

$$A = 16\pi / Re^2. \tag{11.108}$$

In this limit the solution near $\xi = 0$ becomes symmetric in $\theta$, and one can expect an overall solution of the form

$$\lim_{Re \to 0} \Psi[\xi, \theta] = \frac{Re^2}{16\pi} (\sin^2 \theta) g[\xi], \tag{11.109}$$

where the radial function must satisfy

$$\lim_{\xi \to 0} g[\xi] = 2\xi, \qquad \lim_{\xi \to \infty} g[\xi] = \frac{4}{\xi}. \tag{11.110}$$

The corresponding vorticity is of the form

$$\lim_{Re \to 0} \Omega[\xi, \theta] = \frac{Re^2}{16\pi} (\sin^2 \theta) f[\xi]. \tag{11.111}$$

Equations (11.109) and (11.111) are substituted into (11.86), and higher-order terms in the small parameter $Re^2/16\pi$ are neglected. The result is the linear vorticity diffusion equation [the momentum equation in (11.81) with the non-linear terms removed]. Finally we end up with a linear second-order ODE governing the radial vorticity function $f[\xi]$:

$$\xi^2 f_{\xi\xi} + 2\xi \left(1 + \frac{\xi^2}{4}\right) f_\xi + (\xi^2 - 2) f = 0. \tag{11.112}$$

The radial parts of the vorticity function and stream function, $f$ and $g$, are related through the definition of the vorticity,

$$\frac{d}{d\xi} \left( \frac{1}{\xi^2} \frac{d}{d\xi} (\xi g[\xi]) \right) = -\frac{f[\xi]}{8}. \tag{11.113}$$

Equations (11.112) and (11.113) are solved using (11.110), leading to the solution of the Stokes creeping jet:

$$\lim_{Re \to 0} \Psi[\xi, \theta] = \frac{Re^2}{16\pi} \sin^2 \theta \left( 2\xi - \frac{4}{\sqrt{\pi}} e^{-\xi^2/4} - \left( 2\xi - \frac{4}{\xi} \right) \operatorname{erf} [\xi/2] \right). \tag{11.114}$$

### *11.5.2.8 Particle Paths in the Low-Reynolds-Number Jet*

With that background we now consider particle paths of the low-Reynolds-number solution of the jet. Upon substitution of (11.114) into the particle-path equations (11.88) we have

$$\begin{aligned}\frac{d\xi}{d\tau} &= \frac{Re^2}{2\pi}\frac{\cos\theta}{\xi^2}\left(\frac{\xi}{2} - \frac{1}{\sqrt{\pi}}e^{-\xi^2/4} - \left(\frac{\xi}{2} - \frac{1}{\xi}\right)\operatorname{erf}[\xi/2]\right) - \frac{\xi}{2},\\ \frac{d\theta}{d\tau} &= -\frac{Re^2}{4\pi}\frac{\sin\theta}{\xi^2}\left(\frac{1}{2} + \frac{1}{\xi\sqrt{\pi}}e^{-\xi^2/4} - \left(\frac{1}{2} + \frac{1}{\xi^2}\right)\operatorname{erf}[\xi/2]\right).\end{aligned} \tag{11.120}$$

The critical points of (11.120) now need to be located. This is done by setting the right-hand sides equal to zero and solving for the roots. The zeros of the $\theta$-equation occur at $\theta = 0,\ \pi$ for all $\xi$ and at $\xi = 1.7633$ for all $\theta$, independent of the Reynolds number. However, the zeros of the $\xi$-equation depend on $Re$ as follows:

$$Re^2 = \frac{\pi\xi_c^3}{\left(\frac{\xi_c}{2} - \frac{1}{\sqrt{\pi}}e^{-\xi_c^2/4} - \left(\frac{\xi_c}{2} - \frac{1}{\xi_c}\right)\operatorname{erf}[\xi_c/2]\right)\cos\theta}. \tag{11.121}$$

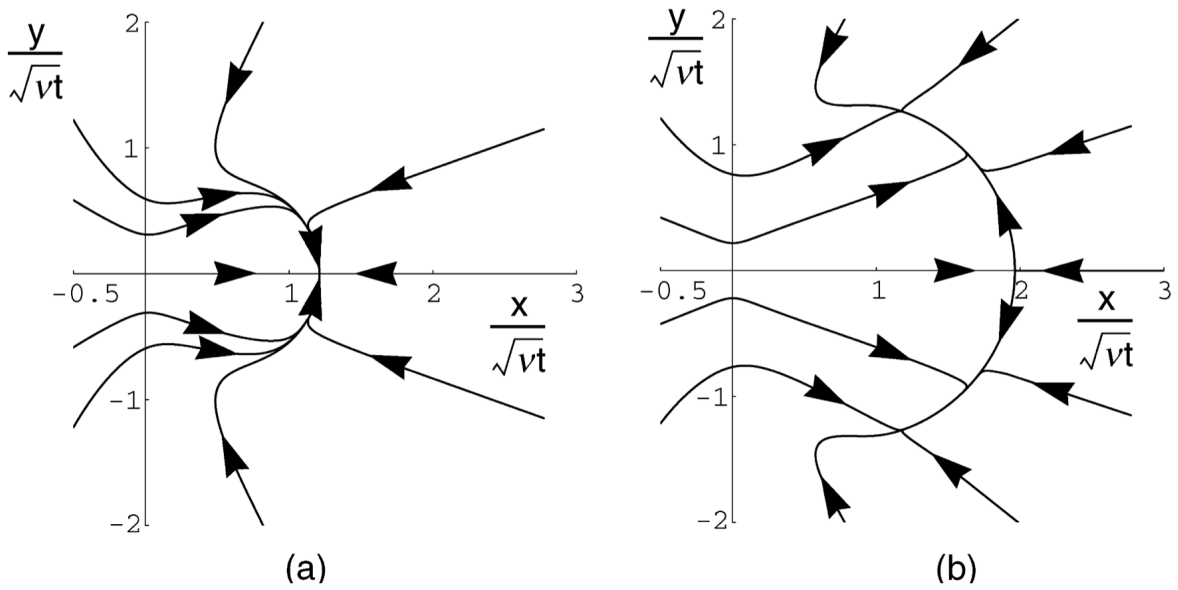


Fig. 11.9. Particle paths for the impulsively started creeping jet at (a) $Re = 4$ and (b) $Re = 8$.

The impulsively started round jet undergoes a bifurcation in the phase portrait of particle paths. For the Stokes solution, the first transition to an off-axis stable node occurs at Re = 6.7806 and the onset of a starting occurs at Re=10.09089.

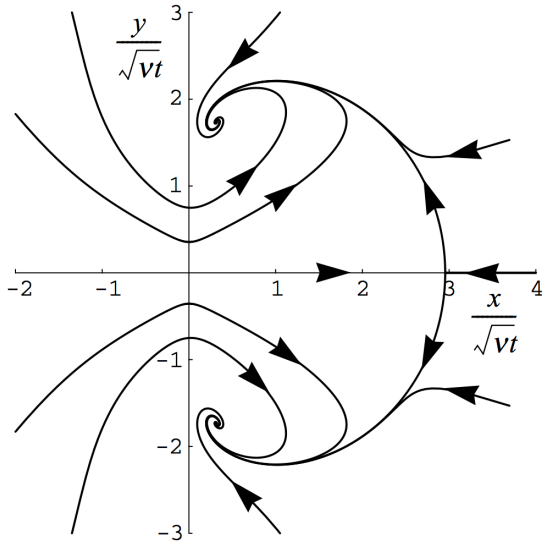


Fig. 11.10. Particle paths for the impulsively started creeping jet at $Re = 16$.

STANFORD
AERONAUTICS &
ASTRONAUTICS

# Streamlines, Vorticity and Particle Paths

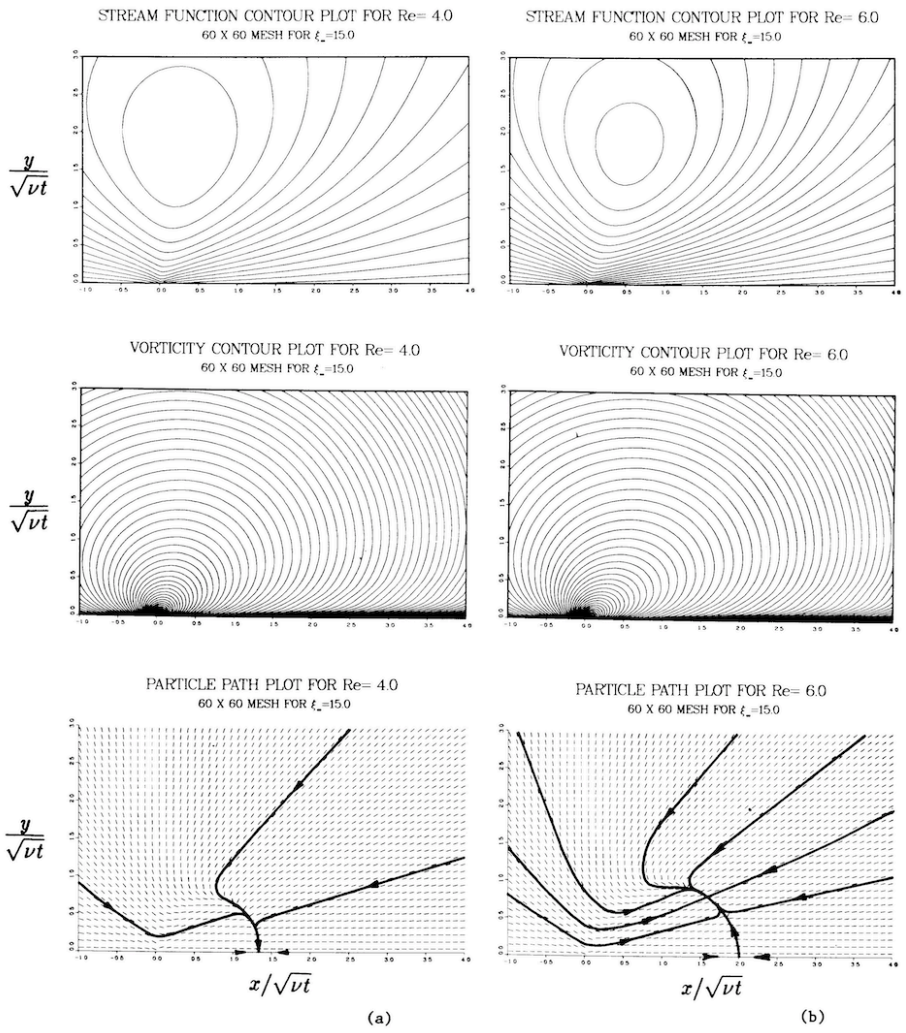


Figure 4. Computed solutions for the round jet at a) $Re = 4.0$ and b) $Re = 6.0$. Quantities displayed are self–similar stream function, vorticity and particle paths.

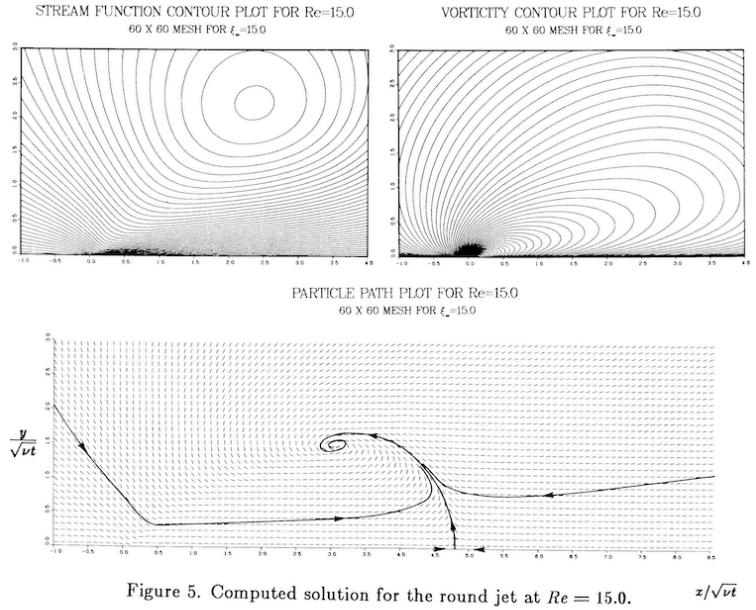


Figure 5. Computed solution for the round jet at $Re = 15.0$.

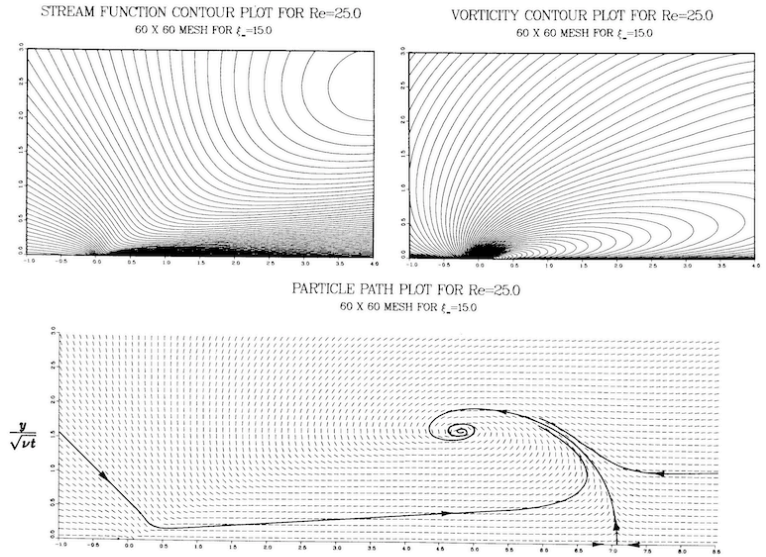


Figure 6. Computed solution for the round jet at $Re = 25.0$.

# Mixing of Material Lines

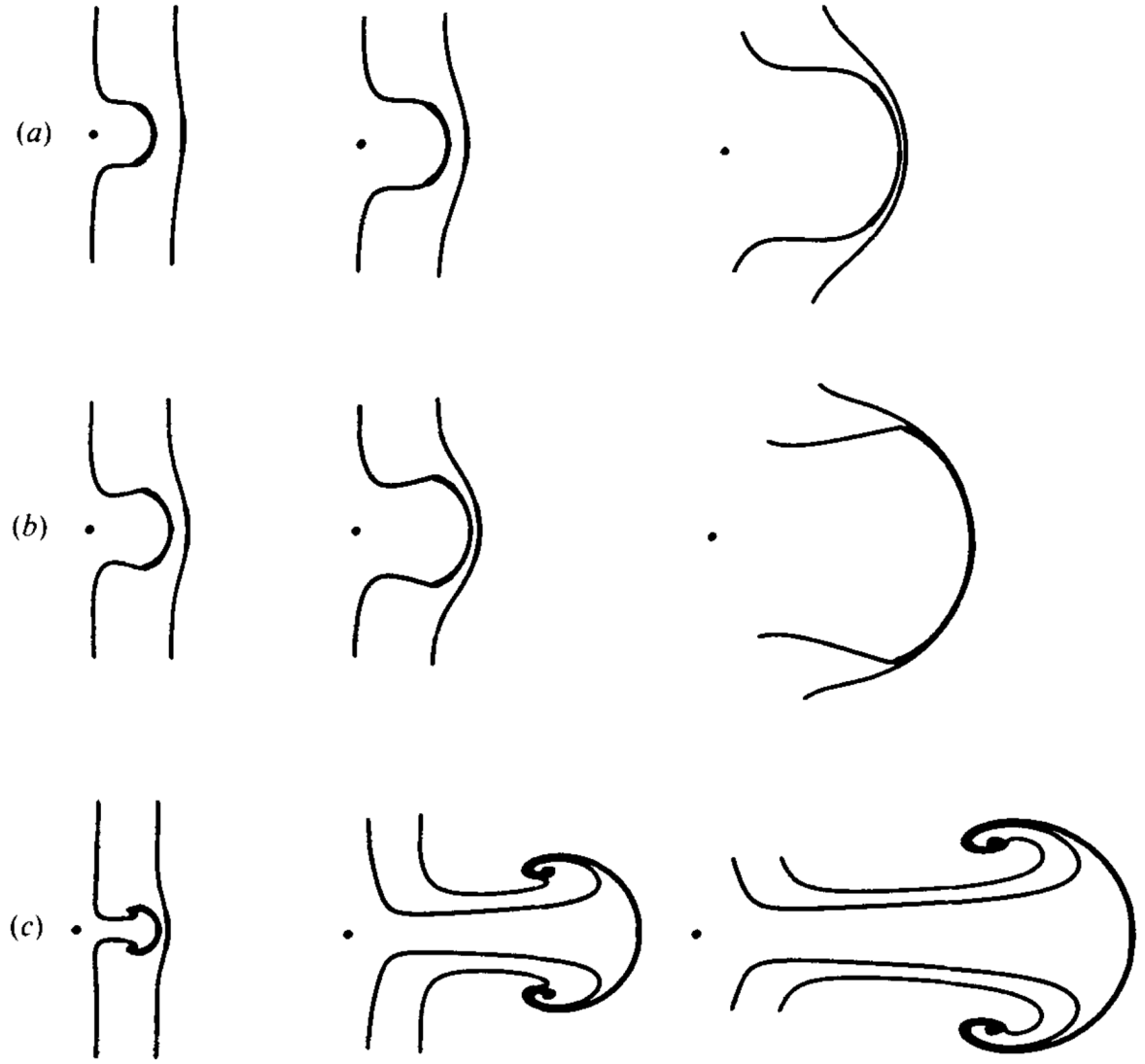


FIGURE 8. Distortion of timelines in physical coordinates under the action of the nonlinear round jet at (*a*) $Re = 4$, (*b*) $Re = 6$, (*c*) $Re = 30$. Time increases from left to right.

# Elliptic Curves

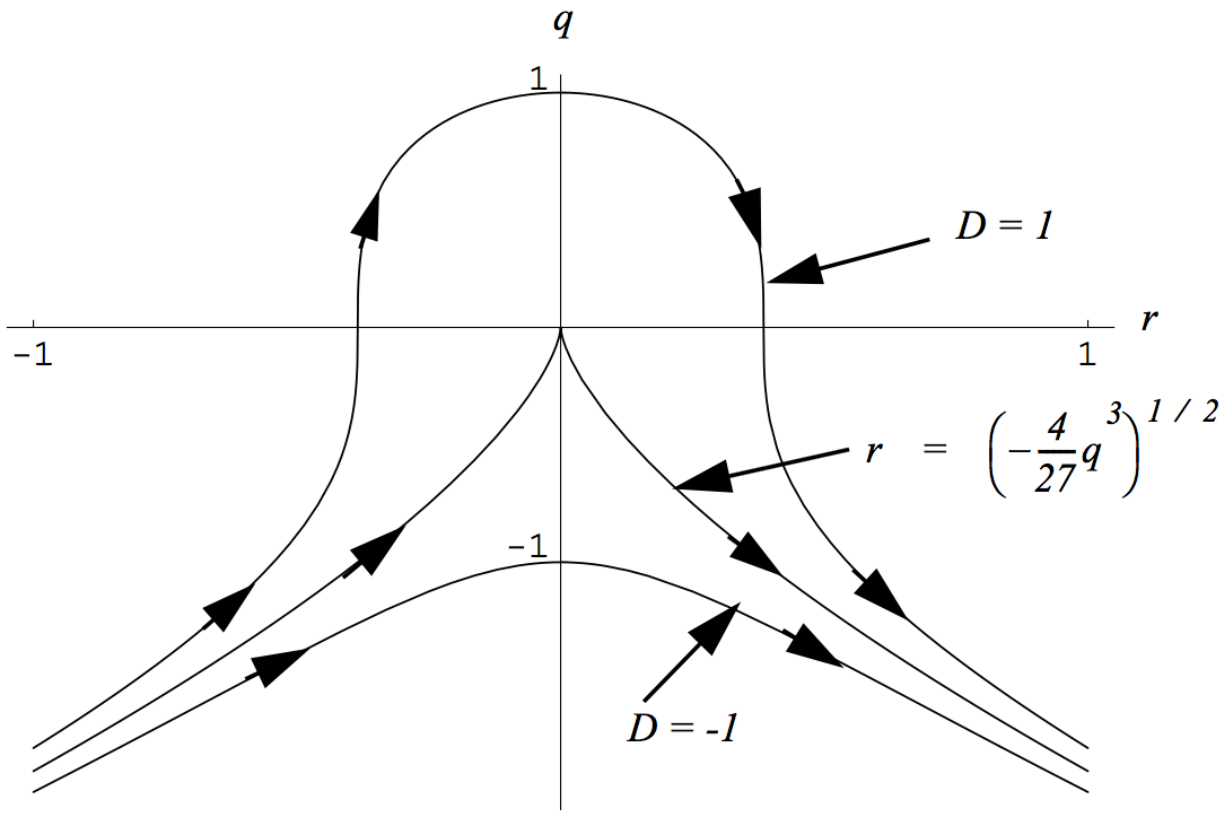


Fig. 6.6. Lines of constant normalized discriminant.

$$D = Q^3 + \frac{27}{4}R^2. \qquad (6.113)$$

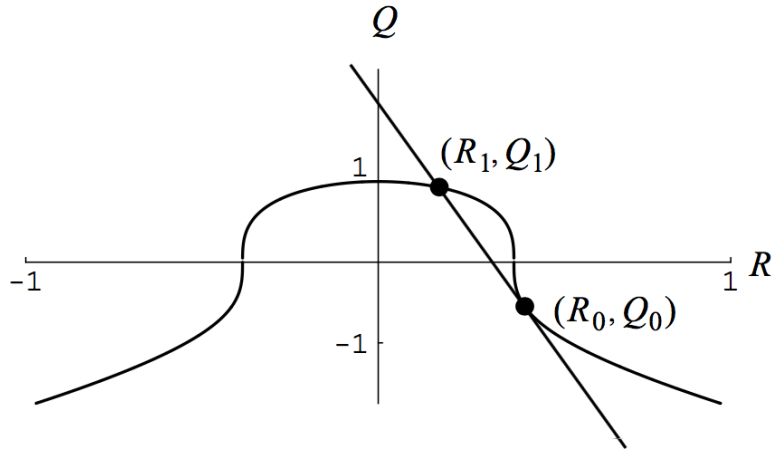


Fig. 6.7. Construction to find rational roots on a curve of constant $D$.

The cubic discriminant has the same value at both points of intersection in Figure 6.7,

$$Q_1^3 + \frac{27}{4} R_1^2 = Q_0^3 + \frac{27}{4} R_0^2, \tag{6.132}$$

and the straight line is of the form

$$R + aQ + b = 0. \tag{6.133}$$

At $(R_0, Q_0)$ the straight line and line of constant $D$ have the same slope as well as the same coordinates. This is used to evaluate $a$ and $b$, and the equation of the straight line is determined to be

$$R + \left(\frac{2}{9}\frac{Q_0^2}{R_0}\right) Q + \left(-\frac{2}{9}\frac{Q_0^3}{R_0} - R_0\right) = 0. \tag{6.134}$$

Now evaluate (6.134) at $(R_1, Q_1)$, and use it to replace $R_1$ in (6.132). The result

is a cubic equation for $Q_1$, which can be factored as

$$(Q_1 - Q_0)^2 \left( Q_1 + \frac{1}{3}\frac{Q_0^4}{R_0^2} + 2Q_0 \right) = 0. \tag{6.135}$$

Two of the roots coincide with the tangent point. The third root, combined with (6.134), leads to the parameterization

$$\begin{aligned} Q_1 &= -\frac{1}{3}\frac{Q_0^4}{R_0^2} - 2Q_0, \\ R_1 &= \frac{2}{27}\frac{Q_0^6}{R_0^3} + \frac{2}{3}\frac{Q_0^3}{R_0} + R_0. \end{aligned} \tag{6.136}$$

It is clear that if $Q_0$ and $R_0$ are rational numbers, then so are $Q_1$ and $R_1$. Repeating the chord–tangent construction at the new root leads to a third rational root, and so on. We shall encounter elliptic curves again in Chapters 11, where we study the geometry of the 3-D flow field of a laminar jet.

All the various bifurcations in the topology of the impulsively started round jet occur at rational values of the invariants of the velocity gradient tensor as well as the acceleration gradient tensor.

# Recall the discussion of 3D vector fields in Chapter 3

For a fixed value of $\lambda$ (3.172) defines a plane in (P,Q,R). As $\lambda$ is varied from $-\infty$ to $+\infty$ the surface D = 0 is created.

Critical points in 3D are characterized by the invariants of a cubic equation for the eigenvalues

$$\lambda^3 + P\lambda^2 + Q\lambda + R = 0, \tag{3.172}$$

$$D = \tfrac{27}{4}R^2 + \left(P^3 - \tfrac{9}{2}PQ\right)R + Q^2\left(Q - \tfrac{1}{4}P^2\right). \tag{3.180}$$

The Cardano surface $D = 0$ is depicted in Figure 3.8. To help visualize the surface it is split down the middle on the plane $P = 0$ and the two parts are

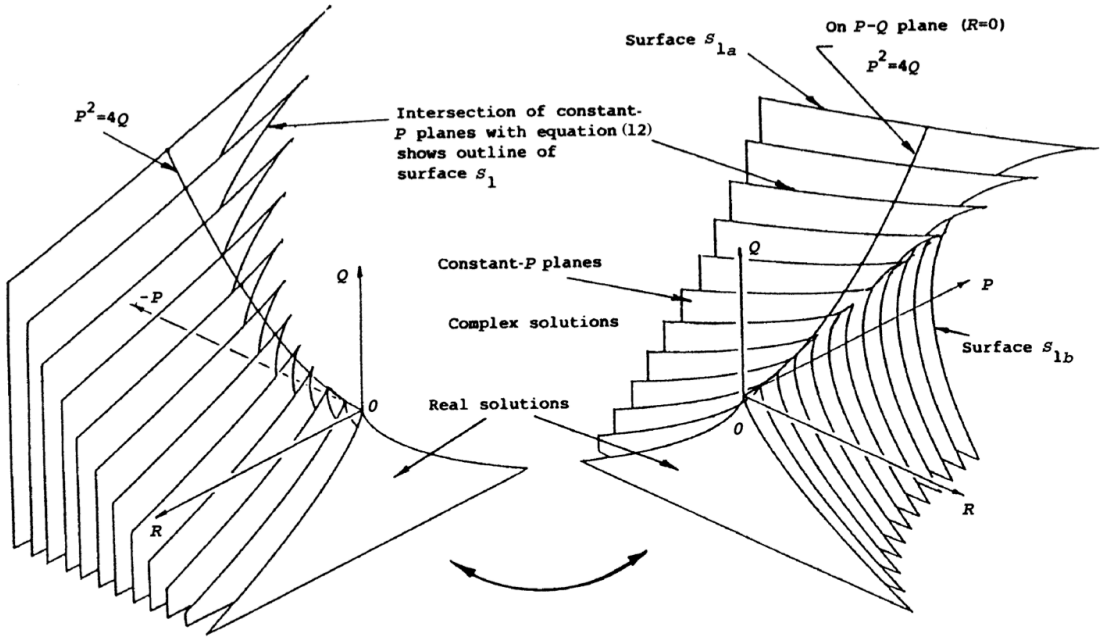


Fig. 3.8. The Cardano surface dividing real and complex eigenvalues in three dimensions (from Reference [3.10]).

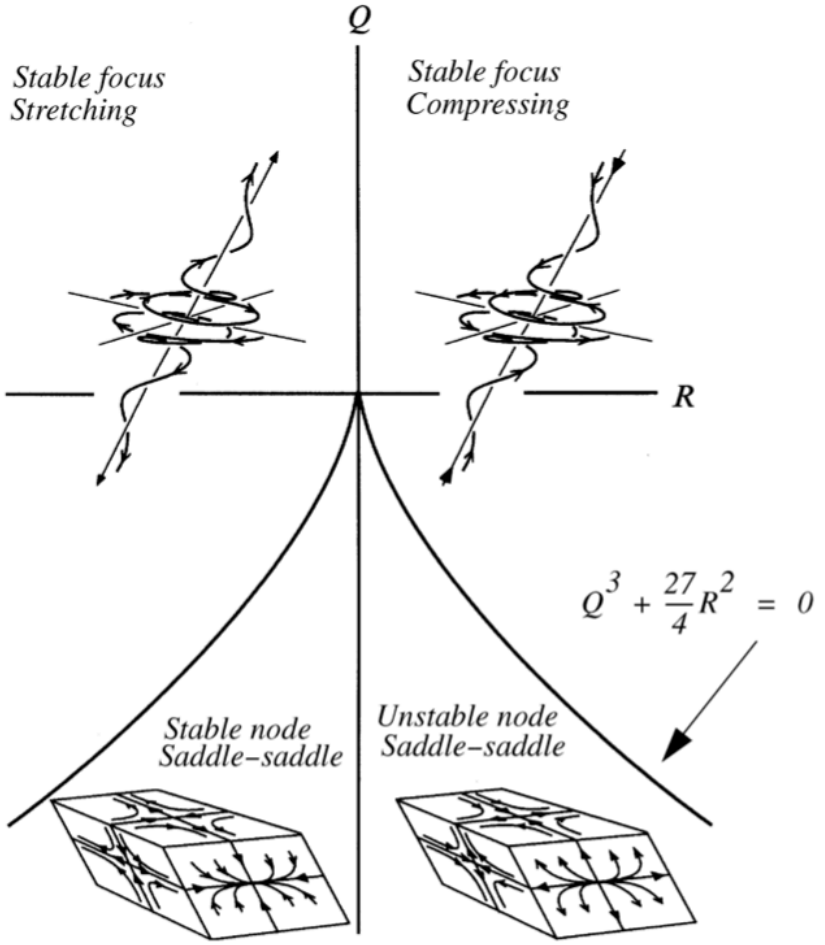


Fig. 3.9. Three-dimensional flow patterns in the plane $P = 0$ (from Reference [3.11]).

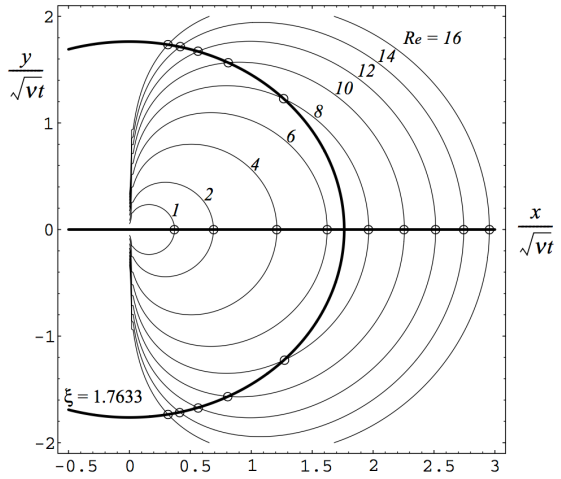


Fig. 11.7. Critical-point locations at several Reynolds numbers for the Stokes jet. The circle has radius 1.7633.

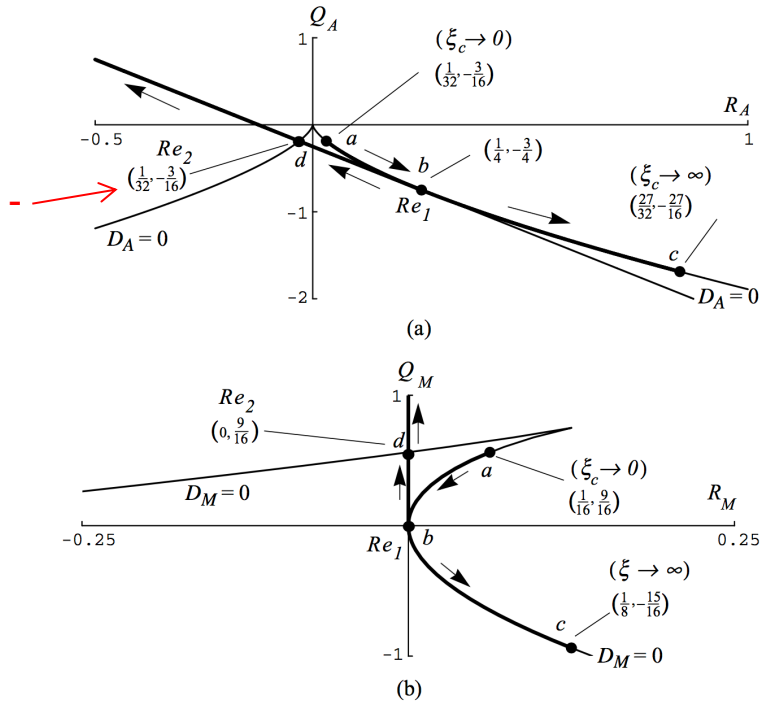


Fig. 11.8. Critical-point trajectories in the round jet: (a) the trajectory in $(Q_A, R_A)$ coordinates at various $Re$; (b) the same trajectory in $(Q_M, R_M)$.

STANFORD
AERONAUTICS &
ASTRONAUTICS

## 11.5.2.9 Invariance of the Vector Field of Particle Paths Relative to a Moving Observer

The self-similarity in time of the jet enabled us to reduce the particle-path equations (11.83) to an autonomous system, (11.88). The invariance of the governing equations under the nonuniform translation group (11.14) can be used to show that, the vector field of particle paths in similarity coordinates is the same for all observers moving with the time scale appropriate to the flow. In Cartesian coordinates the equations for particle paths are

$$\frac{dx^i}{dt} = u^i[\boldsymbol{x}, t], \tag{11.125}$$

which, when transformed to similarity variables, become

$$\frac{d\xi^i}{d\tau} = U^i[\boldsymbol{\xi}] - \frac{1}{2}\xi^i, \tag{11.126}$$

where $\xi^i = x^i/(\nu t)^{1/2}$ and $\tau = \ln t$. In the round jet all length scales vary in proportion to $(\nu t)^{1/2}$. For an observer translating according to this function, the appropriate transformation of coordinates is

$$\begin{aligned} \tilde{x}^j &= x^j + \alpha^j(\nu t)^{1/2}, \\ \tilde{t} &= t, \\ \tilde{u}^i &= u^i + \frac{\alpha^i}{2}\nu^{1/2}t^{-1/2}, \\ \frac{\tilde{p}}{\rho} &= \frac{p}{\rho} + x^k\frac{\alpha^k}{4}\nu^{1/2}t^{-3/2}, \quad \text{sum over } k \end{aligned} \tag{11.127}$$

where the $\alpha^i$ determine the rate at which the observer moves in each of the three coordinate directions. In terms of similarity variables the transformation of velocities and coordinates, (11.127), becomes

$$\begin{aligned} \tilde{\xi}^j &= \xi^j + \alpha^j, \\ \tilde{U}^i &= U^i + \frac{\alpha^i}{2}. \end{aligned} \tag{11.128}$$

In contrast to the velocity vector field, the vector field of particle paths is invariant. To see this we transform the right-hand side of (11.126):

$$\tilde{U}^i - \frac{1}{2}\tilde{\xi}^i = \left(U^i + \frac{\alpha^i}{2}\right) - \frac{1}{2}(\xi^j + \alpha^j) = U^i - \frac{1}{2}\xi^j. \tag{11.129}$$

STANFORD
AERONAUTICS &
ASTRONAUTICS

For the numerically computed nonlinear solution, the first transition to an off-axis stable node occurs at Re = 5.5 and the onset of a starting occurs at Re=7.545.

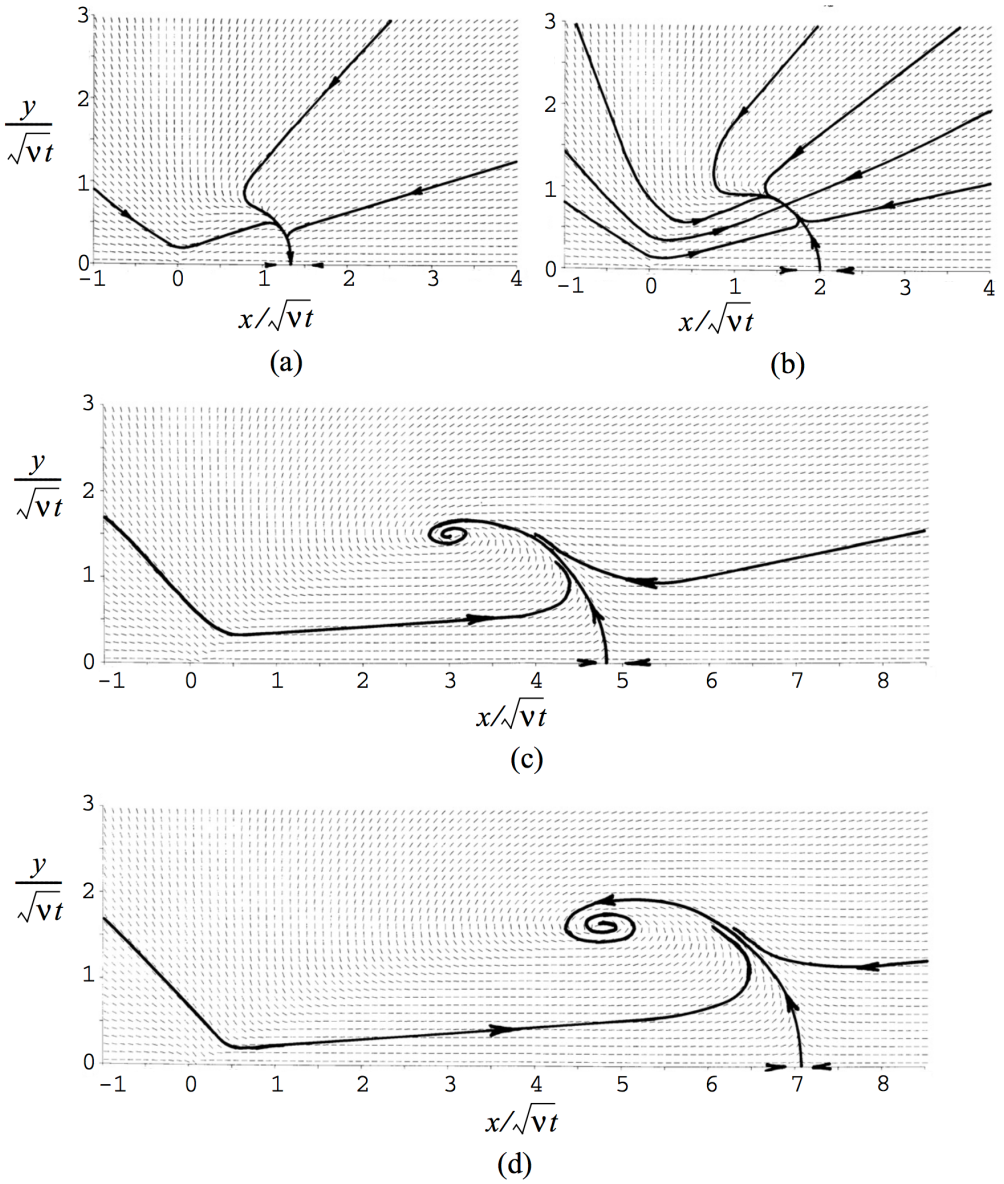


Fig. 11.11. Numerically computed particle paths in the round jet at Reynolds numbers (a) $Re = 4$, (b) $Re = 6$, (c) $Re = 15$, (d) $Re = 25$.

STANFORD
AERONAUTICS &
ASTRONAUTICS